

Airborne Aero-Optics Laboratory – Transonic (AAOL-T)

Jumper, E.J., Gordeyev, S., Cavalieri, D. and Rollins, P.
Dept of Aerospace and Mechanical Engineering
University of Notre Dame

Whiteley, M.R.
MZA Associates Corporation

and

Krizo, M.J.
Dept of Engineering Physics
Air Force Institute of Technology

This paper gives a short background in aero-optics which is the effect that turbulent flow over and around an aircraft has on a laser projected or received by an optical system. The background provides a rationale for developing the Airborne Aero-Optics Laboratory, AAOL, programs. The Airborne Aero-Optics Laboratory-Transonic, AAOL-T, is the second of the laboratory programs having a higher Mach number capability than the original AAOL. This paper describes the AAOL-T operating procedure and capabilities of the flight program. The baseline capabilities capturing wavefronts imposed on a laser beam propagated through the flow fields over the program's morphable optical turret are described as is the method of collapsing the data for more general use. Also described in the paper are the laboratory capabilities and interface guidelines to support other types of testing. Examples of data taken at up to Mach 0.8 are given.

I. Introduction

In the late 1970s and early 1980s optical turrets were extensively studied as the use of high-energy lasers on aircraft became feasible. While the first practical lasers were solid state, like the Ruby and Nd:YAG lasers, for example, but attempting to make them high power was made impossible by the heat-transfer problem which led to thermal stress fractures of the crystal. The heat-transfer problem was solved by creating population inversions from which laser energy could be extracted in high-speed gases so that the thermal energy remaining in the gas could be effectively “dumped” keeping the device from continuing to heat up. The simplest and first truly high-energy gas laser was the Gas-Dynamic Laser (GDL) that achieve population inversion in the vibrational manifold of Carbon Dioxide, CO₂, by first heating the gas through combustion and then passing it through a convergent-divergent supersonic nozzle, cooling its ground state so rapidly that it produced a non-equilibrium vibrational distribution whose upper state relaxed slower than appropriate lower states allowing lasing at several wavelengths, 10.6 μm being the most efficient; the discovery of the GDL made possible placing a high-energy laser (HEL) on board an aircraft and a demonstrator that made use of a KC-135 was developed, the Airborne Laser Laboratory (ALL), and successfully demonstrated the usefulness of airborne high-energy lasers [1].

The ALL used a carbon-dioxide, gas-dynamic laser; but, the laser's long wavelength (10.6 μm) limited its range and intensity on target. From a diffraction-limited point of view the range and intensity of an airborne system can be increased by two orders of magnitude by moving the laser wavelength to 1.0 μm, see Figure 1 [2,3]. In the past 2 decades high-energy chemical lasers moved toward the 1.0 μm mark

with the DF and HF lasers lasing at 3.8 and 2.8 μm , respectively [4], also shown in Figure 1; most notably for chemical lasers, the Chemical Oxygen Iodine Laser (COIL) used on the Airborne Laser (ABL) lased at 1.315 μm [4]. More recently high-energy, solid-state lasers are beginning to become a reality with wavelengths right at 1 μm . As solid-state laser technology and adaptive-optic systems continue to improve, the use of lasers for directed energy and communication applications has taken on new life; however, the shorter wavelengths (1-1.5 μm) of these new lasers are more affected by the inhomogeneous refractive mediums surrounding the aircraft [2,3]. When the source of the inhomogeneous refractive medium is due to the turbulence in the flow over and around the turret on an airborne platform, the problem is referred to as “aero-optics” [2,5,6] and its presence imposes an opposite effect on range and intensity from that of the diffraction-limited enhancements of the shorter wavelengths, as can be seen in Figure 2 [2,3]. For the ALL, aero-optics posed only a 5% reduction in diffraction-limited performance.

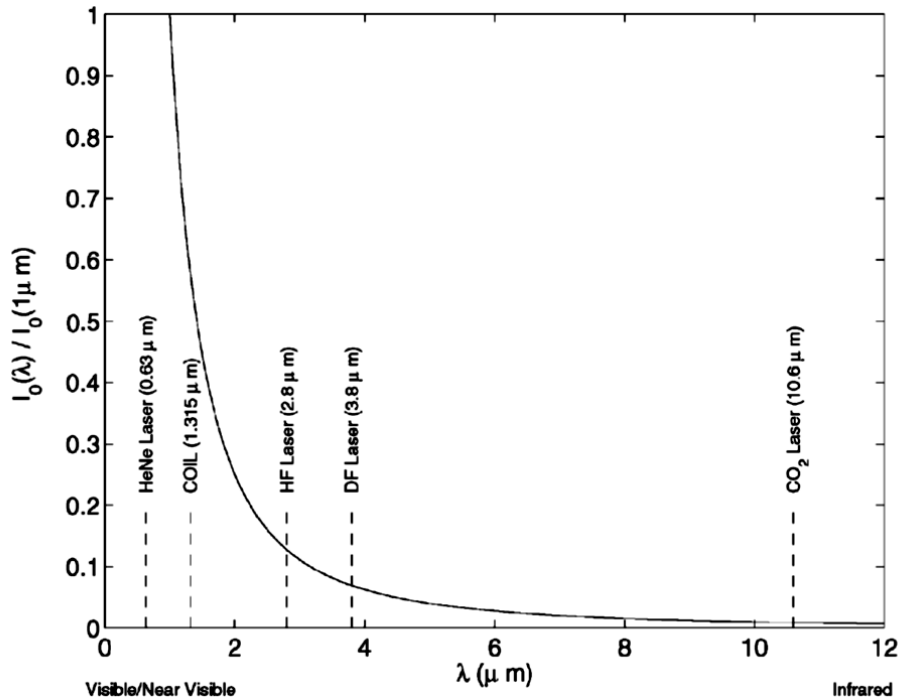


Figure 1. The diffraction-limited, on-axis Intensity for a given aperture size and range of a laser as a function of wavelength, λ , divided by that at 1 μm [2,3].

Because the aero-optic effects on ALL were estimated to be 5% or less, by the end of the 1980’s all funding for research in aero-optics had come to an end and system designers took this as reassurance that overall system impact of aero-optics on airborne-laser performance could always be estimated as being 5% or less, regardless of laser wavelength; on the other hand, the physics, as shown in Figure 2, said otherwise. The plot in Figure 2 is based on the large-aperture approximation [7,8], where the Shrehl ratio, SR, the ratio of actual line-of-sight intensity, I , to the diffraction-limited intensity, I_o , can be approximated as,

$$SR = \frac{I}{I_o} = e^{-\left(\frac{2\pi \cdot OPD_{rms}}{\lambda}\right)^2} \tag{1}$$

where OPD_{rms} is the spatial root-mean-square of the optical path difference and λ is the laser wavelength. An OPD_{rms} reducing SR by 5% at 10.6 μm becomes a serious problem when the wavelength is reduced by ten as can be seen in Figure 2. While the atmosphere is also an inhomogeneous refractive medium and thus the effect of the atmosphere is also exacerbated by the shorter wavelengths, the spatial and temporal frequencies associated with aero-optics are far higher than those due to the atmosphere and so adaptive-optic mitigation approaches are much more difficult to develop. The consequence of aero-optics for the shorter wavelengths effectively limits the laser-system's field of regard, and yet a large field of regard is essential to making airborne laser systems practical for directed energy and free-space communication.

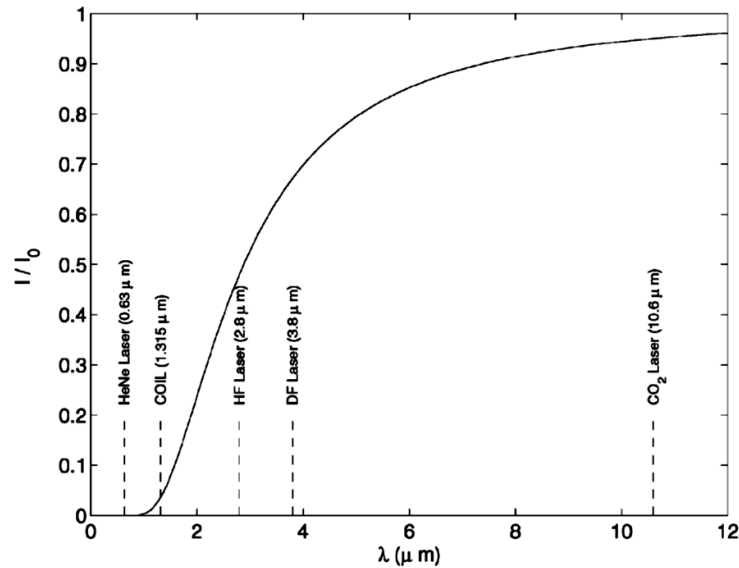


Figure 2. Ratio of actual on-axis intensity to diffraction limited intensity due to OPD_{rms} level that would produce a 95% ratio at 10.6 μm [2,3].

Although, the physics would dictate the importance of optical turbulence in the flow over the exit pupil of a laser on an airborne system, even the idea that the reduction in GDL performance would be as high as 5% was brought into question in the work performed prior to the 1990's and a statement was even made that the OPD_{rms} at 40,000 ft for a Mach 0.8 aircraft would be less than 0.1 μm , having "measured it." One would think that the prior research in aero-optics in the 1970's and early 1980's would be directly transferable to the new interest brought by the new shorter-wavelength high-energy lasers, but it is not, primarily due to the methods used then to estimate the density fluctuations. The reason for the error was the use of hot-wire measurements of the flow field from which a linking equation was used to infer OPD_{rms} [2,5].

A research initiative by AFOSR in the mid 1990's reinstated funding for aero-optics based on the recognition that aero-optics might be important to shorter-wavelength airborne laser systems. Early work under this initiative produced the first truly-high-frequency wavefront sensor, the SABL sensor which operated at 100+ kHz [9], and its serendipitous application to laser propagation through a Mach 0.8 separated shear layer at Arnold Engineering Development Center (AEDC) [10,11]. The AEDC wavefront measurements demonstrated two important facts: the first was that the aero-optic problem was much larger than had been presumed; and second, the cause of the aberrations was not understood. These facts led to continued support for aero-optics research that eventually led to a rational basis for the cause of the aberrations [12] and also documented aero-optical effects on various-geometry turrets of interest and

research into mitigating the effects through flow-control approaches, adaptive-optic approaches, combinations of these, as well as interest in being able to predict these effects using computational fluid dynamics. Still until only a few years ago, all of the experimental work was performed in wind tunnels. The increased interest in aero-optics also led to continuous improvements in wavefront sensing capabilities and instrumentation.

Six years ago, the High-Energy Laser, Joint Technology Office (HEL JTO) recognized the need to evolve the study of aero-optics to in-flight research and thus was created the Airborne Aero-Optics Laboratory (AAOL) Program which made use of two Cessna Citation Bravos. The original AAOL program was extremely successful and the Citation configuration and capabilities are detailed in Reference [13]. Advances in aero-optics making use of the AAOL wavefront data have greatly advanced the knowledge of the physics and mitigation of aero-optical environments. The original program was so successful that a follow-on AAOL program was begun with the requirement that the Mach numbers had to be increased to Mach 0.8+ and changed the program name to Airborne Aero-Optics Laboratory – Transonic (AAOL-T). To meet the Mach 0.8+ requirement the program to migrated to Falcon 10's.

Flow over a hemispheric turret goes supersonic for incoming flows above Mach 0.55; once the flow is supersonic it shocks and causes the flow to separate from the turret forming free shear layers. In the previous AAOL program we were able to fly up to Mach 0.7 and as the Mach number increased above 0.55, the shock phenomena and associated fluid mechanics changed with increasing Mach number. We had been able to examine the low end of this transonic range in wind tunnels, but attempting to test in wind tunnels at Mach numbers of 0.8 and above becomes increasingly difficult. On the other hand, as we learned in the Citations and now in the Falcons, testing at these Mach numbers is no more difficult than at the lower Mach numbers, so apart from the importance of doing in-flight testing, from a practical point of view, flight testing at the higher Mach numbers is much easier in flight.

This paper describes the AAOL-T operational concept and, in as much as possible, describes the experimental set up of the source and laboratory aircraft, as a reference for other papers that will make use of data as it becomes available. To this end, the paper begins by describing the major differences between the AAOL and the AAOL-T starting with the concept and then the implementation. Also included is a description of wavefront sensor instrumentation used on the laboratory aircraft and the scaling laws that allow the data to be generalized.

II. Concept

The objective of both the AAOL and the AAOL-T programs is to obtain aero-optic data in flight. As such, the approach to both programs are similar: a source laser beam leaves the source aircraft as a small diverging beam with a beam diameter of a few millimeters which then diverges to overfill the pupil aperture on the laboratory aircraft turret. The usual formation flight distance from exiting source beam to the laboratory's turret pupil is 50 m. As mentioned above, the AAOL program used Citation Bravos while the AAOL-T uses Falcon 10s. In the Citation laboratory aircraft, a 12 inch diameter turret described in Reference [13] protruded into the slip stream on the starboard side of the Citation through a highly-modified emergency escape hatch just aft of the right seat of the cockpit. The turret was firmly mounted to a large optical bench which was in turn mounted to the seat rails on the starboard side of the aircraft. In the Falcon 10 the emergency escape hatch is over the wing so that if the turret were mounted through it, as in the Citation, the field of regard of the turret would be greatly reduced by the wing and engine nacelle. Some consideration was given to modifying the frame of the aircraft with a hole just aft of the cockpit right seat in a similar location to where the turret was mounted on the Citation; however,

further analysis led us to modifying the upper clamshell of the crew entry door. The required modifications are covered in a later section. Figure 3 shows a schematic of the formation approach and Figure 4 shows a photograph taken from the source aircraft in flight.



Figure 3. Schematic of the AAOL-T formation approach with two Falcon 10s flying in formation at a separation distance of 50 m.



Figure 4. View of the Laboratory Aircraft from the Source Aircraft with the turret aperture illuminated by the diverging source laser.

From Figure 3 it is clear that the most obvious difference between the AAOL and the AAOL-T is the fact that the turret now protrudes into the airstream on the port side of the aircraft. This required the original AAOL turret to be modified which required rebuilding the optical component box to allow the incoming beam to point aft on the bench on the port side of the aircraft. The required modification allowed for some upgrades in the turret performance which will be covered in a later section.

III. Falcon 10 Modifications for the Laboratory Aircraft

The primary modification of the Laboratory Aircraft was the construction of a new crew entry door. Unlike the AAOL program the AAOL-T program has as an additional objective the support of other programs and other turret configurations. From the start the AAOL-T planned on testing a Lockheed-Martin (L-M) turret so the door modifications were designed to be able to accommodate the L-M turret as well as a variety of envisioned turrets by designing a large opening and making use of turret specific interface plates. The standard main, crew entry door of Falcon 10's is made of two halves in the form of a clamshell design. The upper half rotates upward and the lower half rotates downward as seen in Figure 5, Left.

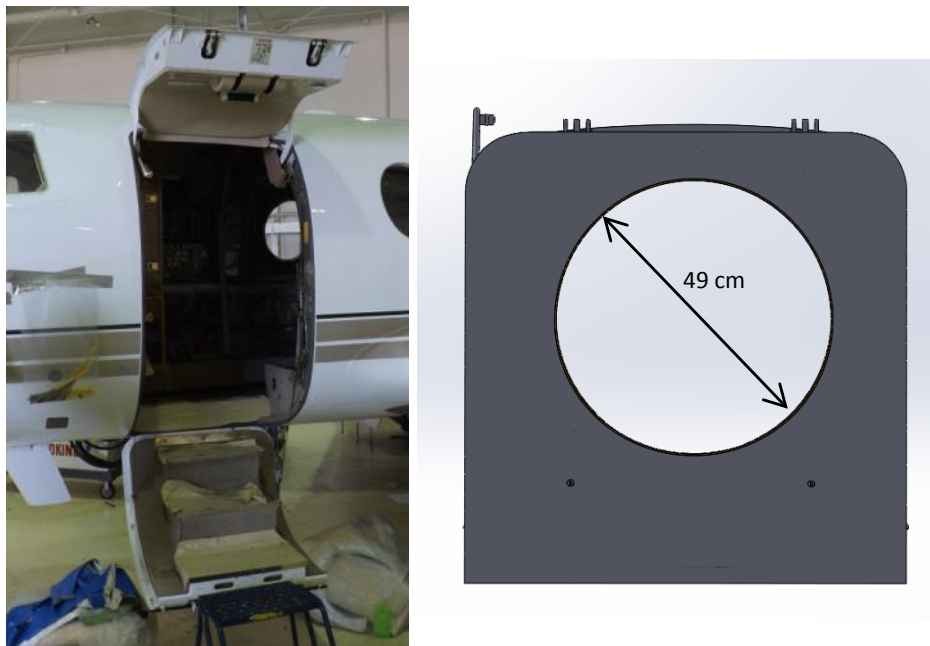


Figure 5. Left: Clamshell main door fully opened with top and bottom halves shown; Right: Outside view of modified door with 49cm diameter opening.

The upper half of the door has redesigned to accommodate turrets with diameters of up to 49cm (19.2"). See Figure 5, Right. The inside of the door has an interface ring permanently mounted to it which has a 49cm diameter opening in it (see Figure 6, Left). The interface surfaces that can come into contact with turret hardware are smooth surfaces. The L-M turret, for example, has an O-ring on its surface which comes into contact with one of the interface surfaces of the ring making an air-tight seal. The mounting hardware for the 12" diameter AAOL-T turret includes an interface plate with a 35.5cm diameter (14") opening, see Figure 6, Right. Any other turret to be flown in the AAOL-T would either directly seal to the permanently-mounted ring or have a tailored interface ring manufactured for it. The AAOL-T interface plate has an O-ring which makes an air-tight seal against the interface surface of the permanent ring (see Figure 7).

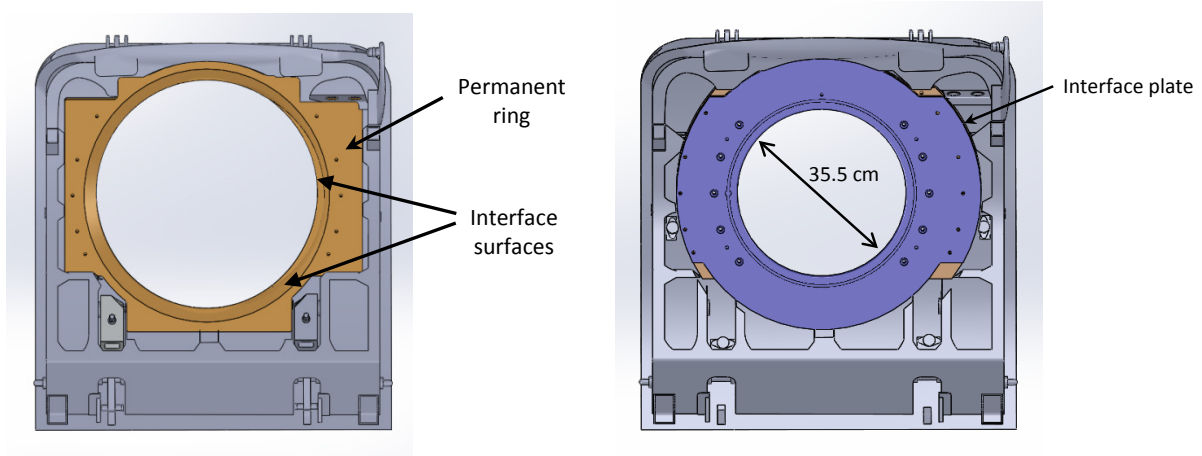


Figure 6. Right: Inside view of door with permanently-mounted ring and interface surfaces; Right: Inside of door with interface plate

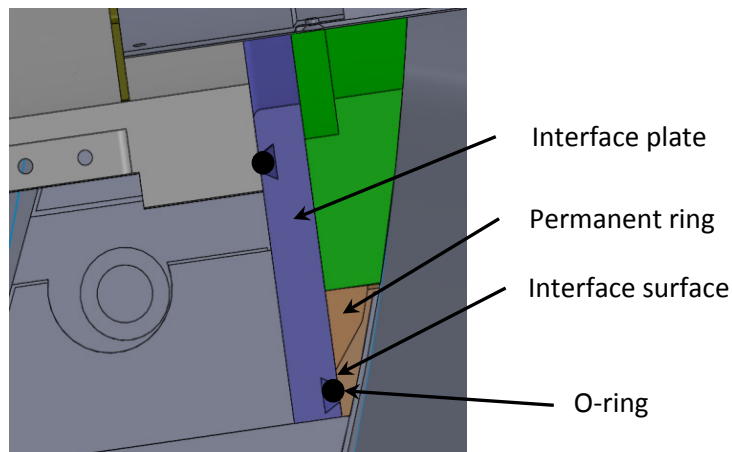


Figure 7. Partial cross-sectional view of door assembly as seen looking from nose to tail of aircraft.

Different interface plates can be made for turrets of different sizes to the interface ring. For example, the interface plate for the AAOL-T turret has a 14” opening to accommodate the 12” diameter turret. The inch spacing between that turret and its interface plate is filled with a rubber grommet. Any new turret can have its own interface plate. The interface plates simply need to have an O-ring that makes contact with the smooth surfaces of the permanent ring in order to create an air-tight seal. Engineering drawings and digital solid models are available to use in the design of new hardware such as interface plates for new turrets.

In addition to the door modifications, high-pressure air tanks have been installed in the Laboratory Aircraft for use in active flow control experiments. Details on the air supply specifications and interface requirements can be made available to potential users, but suffice to say that air is available and has been used for in-flight active flow control experiments. Laboratory 110 V power is also available. 3 Cotek SK1500-124 pure sine wave inverters @ 1500 watts continuous have been installed in the aircraft pulling power by equally splitting their power between the two main engine generators.

III. AAOL Turret Modifications and Upgrades

As mentioned in Section II, the baseline AAOL turret was developed to protrude from the Citation Bravo on the starboard side of the aircraft into the airstream from the emergency escape hatch just aft of the pilot right seat. For the reasons discussed in Section II the turret was modified to protrude into the airstream on the Falcon 10 on its port side (see Figure 8, Upper Left). The port side modifications also required that the beam had to exit the turret and optical box assembly on the opposite side of the turret so as to point aft from the assembly as shown in the figure. This required the optical components including the curvature removal telescope and fast-steering mirror to be moved as shown in Figure 8, Upper Right. In addition, the fixed focus on the acquisition camera, also shown in Figure 8, Lower, was set at a nominal 50 m by adding a lens in front of the original camera lens. It should also be noted that the spherical curvature imposed on the beam (see next section) is removed from the incoming beam in the optical path prior to incidence on the fast-steering mirror; along with refined spherical removal using the data from the differential GPS system described below, the remaining spherical curvature is due to the mean aerodynamic lensing imposed by aero-optic effects.

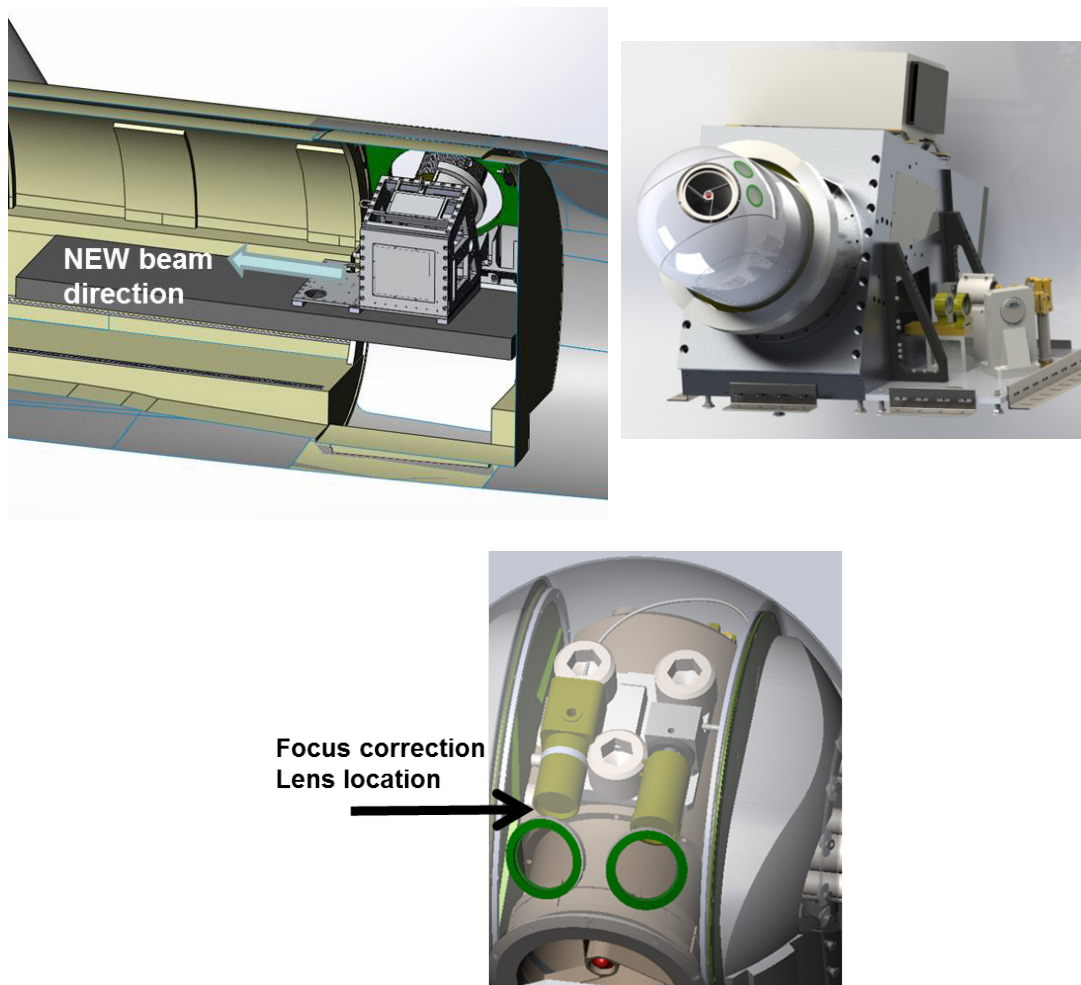


Figure 8. Upper Left: Falcon 10 location for baseline AAOL Turret; Upper Right: New Optical Box; Lower: Acquisition Camera Correction Lens location.

Jitter Control Tuning. In addition to the mechanical and optical modification to the turret, the fine steering mirror controller was tuned to improve the residual jitter on the beam as it exited the optical box onto the optical bench over that experienced on the old AAOL turret configuration. Although jitter is usually removed from the data in post-processing, actual jitter data has been used in the past for jitter prediction experiments that depend on external turret mold lines and flow-control schemes. With the tuned configuration on the jitter control, wind-tunnel tests of the turret under load were performed and exercised the jitter control states in the turret system. Figure 9 shows a back-sum of the measured jitter from the wind tunnel tests at two turret pointing angles corresponding to the locations where the highest jitter levels were previously noted. The coarse track was measured, and then the system was placed in fine track. The back-sum plot of the system jitter illustrates that the fine track control has the desired feature of greatly reducing the jitter level at frequencies below 500 Hz, essentially eliminating jitter contributions noted in the coarse track below 100 Hz. The system control amplifies the jitter features at 600 Hz and 950 Hz which are due to the primary mirror and a resonance in the fast-steering mirror. Jitter control behavior in fine-track is nearly equal for both pointing angles measured. Due to limitations in the existing controller hardware, we've made no attempt to design a controller which would eliminate the known high-frequency jitter features. The 21 μ rad of jitter measured with fine track control engaged is lower than typically observed during wind tunnel testing and satisfactory for science wavefront sensor operation during AAOL-T flight tests.

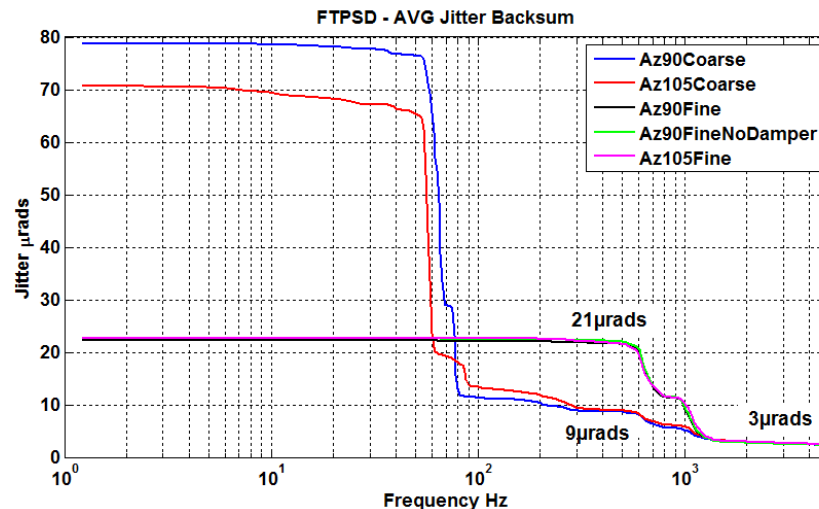


Figure 9. Assessment of jitter control loop closure during wind tunnel loading after tuning of the jitter control system.

IV. Source Laser System and Differential GPS System

Source Laser Tracking System. The laser source for AAOL-T mentioned above is an improvement to the system used in AAOL program [14]. The redesign of the mounting hardware to fit in the Falcon 10 afforded the opportunity to improve several aspects of the AAOL source system. The first was the removal of the vibration dampers and replacement with a rigid mounting. It was observed in the AAOL program that the source aircraft vibrations did not require the use of dampers. By eliminating the movement of the dampers, the laser source system was able to be mounted closer to the aircraft window and use sliding rails to reposition the system to capture different angles. There is now $\frac{1}{4}$ " between the source Aerotech gimbal steering mirror and the aircraft window instead of 2"-3" in AAOL program. This

improved the Field of View (FOV) of the source out to 70° away from the window normal. This proved to be a crucial step in improving the FOV of the experiment in general. Figure 10 shows a rendering of the laser source installed in a cutaway Falcon 10. This shows the sliding rails as well as the installation of the necessary equipment.



Figure 10. Rendering of Laser Source Installed in Falcon 10 Showing Sliding Rails, Equipment Mounting and Operator Location.

Additionally, the usability of the system was greatly improved with the incorporation of a second camera. In the AAOL program’s system the track camera was also used as an acquisition camera. This meant that initiating tracking required stopping the camera, changing settings and restarting its acquisition. This resulted in problems where upon restarting the camera the AAOL turret was not visible and tracking failed. By adding a second dedicated camera for acquisition the system can be manually steered in wait to track mode until the track camera sees its target and automatically initiates tracking. The addition of the new camera allowed the source laser tracking system’s performance to be retuned and refined. Figure 11 shows the improvements to Error Rejection Transfer Function (ERTF) with the new camera. The biggest improvement lies in the intermediate frequencies from 1-10Hz where much of the disturbance power is.

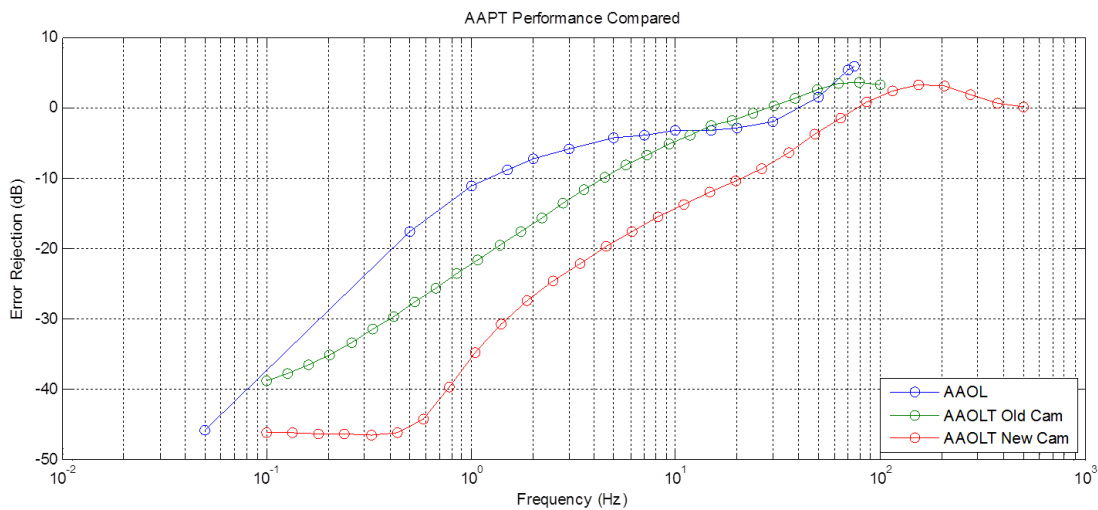
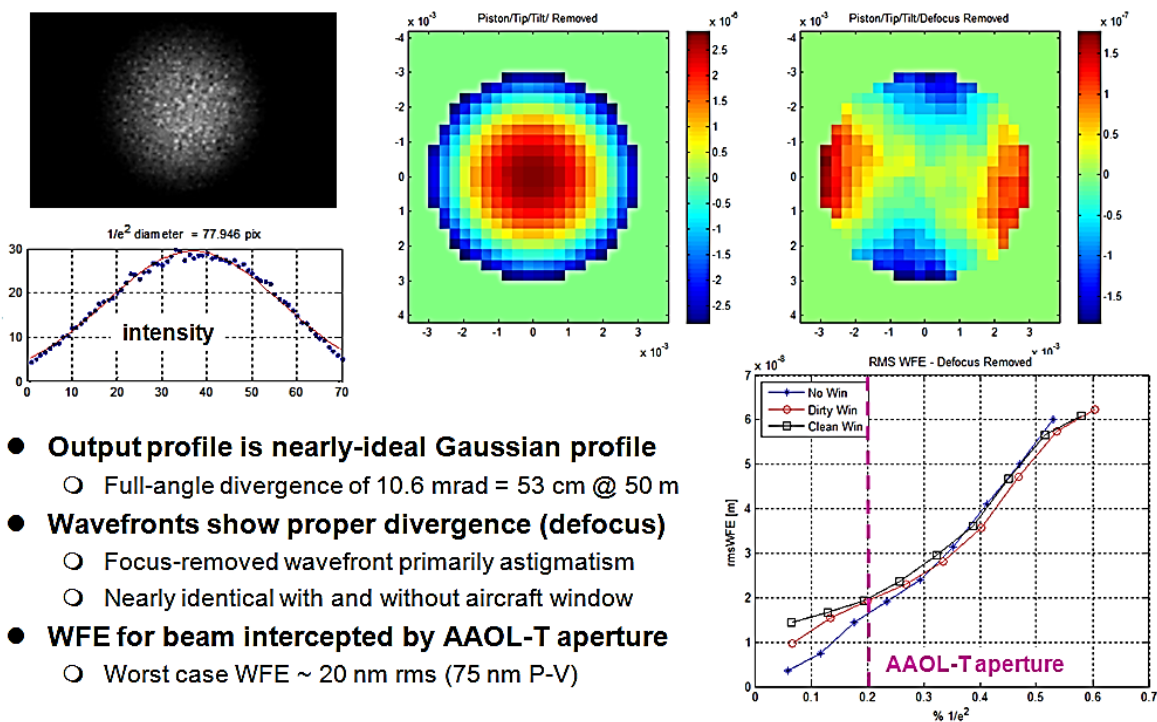


Figure 11. Error Rejection Transfer Function (ERTF) for the Laser Source in AAOL, Retuned with the Old Camera and With the New Camera.

Differential GPS System. A GPS system has been in place since the AAOL program to accurately measure the range between the source and the turret pupil in order to remove range induced focus error from aero-optic induced focus error. Both aircraft have a GPS receiver and antenna installed. In the AAOL program this data was intermittent due to a number of factors. For AAOL-T the GPS antenna was mounted on the roof of the aircraft instead of placing them in the cockpit window. This gives a nominal view of satellites. Additionally, an amplifier was placed between the antenna and the GPS receiver to provide the receiver with the expected signal levels. Lastly the GPS units have to share data to compute the difference in position. In AAOL this was done with a Wi-Fi link between the two planes. For AAOL-T, a new radio set that provided higher power and more control of the data rates was added. The combination of these things has allowed >99% reliability in range when the aircraft are in position.

Source Laser Characterization. Transition to flight testing on the new AAOL-T program also involved transitioning to a new laser source. The new laser had to be characterized. Figure 12 shows the key divergence and wavefront measurements made to characterize the laser.



- **Output profile is nearly-ideal Gaussian profile**
 - Full-angle divergence of 10.6 mrad = 53 cm @ 50 m
- **Wavefronts show proper divergence (defocus)**
 - Focus-removed wavefront primarily astigmatism
 - Nearly identical with and without aircraft window
- **WFE for beam intercepted by AAOL-T aperture**
 - Worst case WFE ~ 20 nm rms (75 nm P-V)

Figure 12. AAOL-T Source Characterization Measurements.

The new source laser has a nearly ideal Gaussian profile. The full-angle divergence (e^{-2} intensity) of the beam was 10.6 mrad, which equates to 53 cm at 50 m range between source and laboratory aircraft. After removing the focus (divergence) term from the wavefronts, we found a residual which is dominated by astigmatism, as shown in Figure 12. For the beam intercepted by the AAOL-T aperture, the rms wavefront error associated with the source itself was determined to be approximately 20 nm. Since most of this will be static wavefront error which is removed from the primary wavefront error measured on AAOL-T, this level of source wavefront error has essentially no impact on the AAOL-T science wavefront measurements.

V. Field of Regard

The new placement and the arrangement of the exterior mold line of the Falcon actually increased the azimuth and elevation ranges available on AAOL. The definition of azimuthal direction is given in Figure 13 and a diagram of achievable elevation and azimuthal angles is given in Figure 14. The region above the green line corresponds to the laser beam being within 70 degrees, relative to the line normal to the laser plane window; above this angle the laser intensity and quality rapidly goes down due to the very shallow angle through the source aircraft window. Essentially all positive azimuthal angles are achievable, except for azimuthal angles larger than 150 degrees at low elevation angles. These shallow angles cause the laser beam to be clipped by the laboratory aircraft wing. Negative azimuthal angles are mostly unreachable due to beam blocking by the laser aircraft wing. A detailed description will be in the paper.

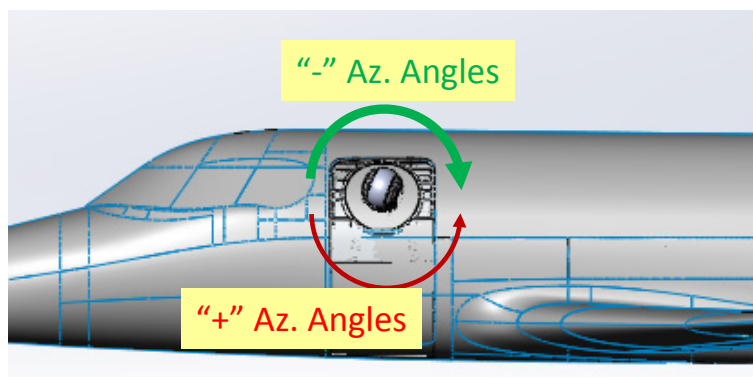


Figure 13. Definition and direction of turret azimuthal angle.

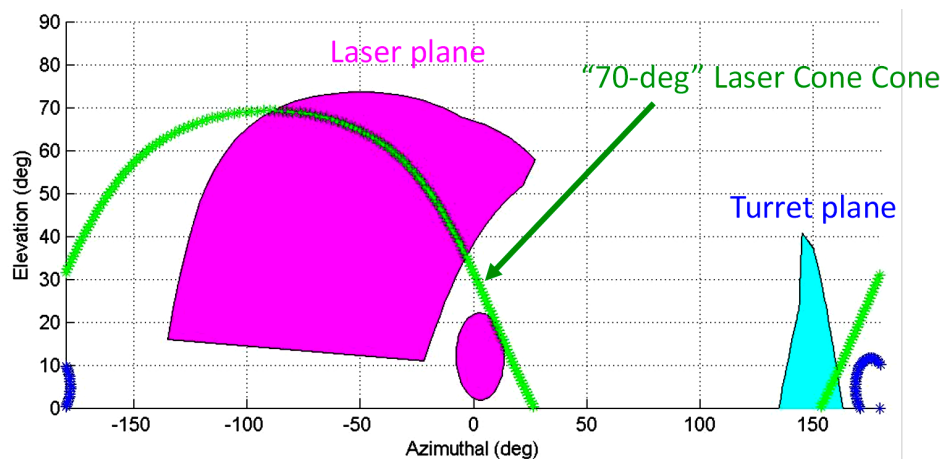


Figure 14. Diagram of achievable elevation and azimuthal angles on AAOL-T.

VI. Instrumentation

Figure 15 shows a schematic of the optical setup in the laboratory aircraft. After the beam is stabilized using a closed-loop fast-steering mirror (FSM) system, discussed in Section III, wavefront measurements are performed using a high-speed Shack-Hartmann wavefront sensor. In its baseline configuration the sensor uses 32x32 subapertures and a frame rate of up to 25 kHz. Simultaneous with the 2-D wavefronts, the beam jitter is also measured by splitting the incoming beam and focusing it on a

position sensing device. The jitter is acquired with the turret viewing angle and FSM position information at 25 kHz. Figure 16 shows a photograph of the optical system installed in the Falcon 10. Flight conditions are also obtained simultaneous with the wavefront and jitter measurements from on-board Pitot probe, installed on the opposite side of the laboratory aircraft. The aircraft separation is continuously measured throughout the flight using a differential GPS system with the accuracy of less than one inch.

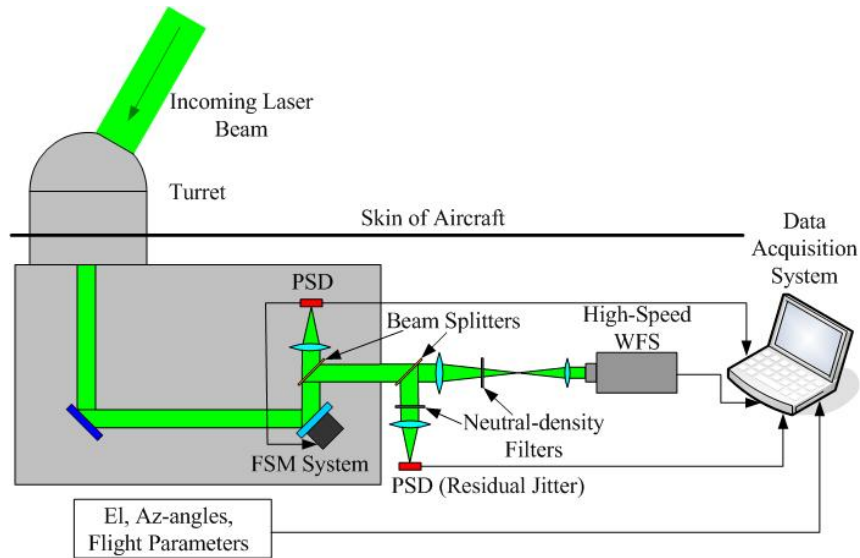


Figure 15. Schematic of the optical setup.



Figure 16. View of optical bench inside the AAOL-T

VI. Other Capabilities

The AAOL-T was also designed to perform more than just data collection for post processing. As such, for example, special features have been designed into the AAOL-T to support active and passive flow control experiments. Another capability of the turret is that it can be modified, morphed, to be a canonical hemisphere-on-a-cylinder type geometry or recessed to a hemisphere or less; the window over the aperture can be either conformal or flat. In its baseline form the turret contains “smiles,” i.e., two crescent shaped volumes, to accommodate a full aperture at 0.0 and 180 degrees elevation; however, these smiles can be modified by adding fill to the open volumes, see Figure 17, Left. In the modified state these open volumes are covered by rolled sheet metal which is screwed to the outer surface of the cylindrical base. The open volumes are filled-in with aluminum pieces which conform to the shape of the contours of the cylindrical base and the sphere and are screwed to the covers, see Figure 17, Right. This modification still allows for the elevation angle to rotate within its full range of motion.

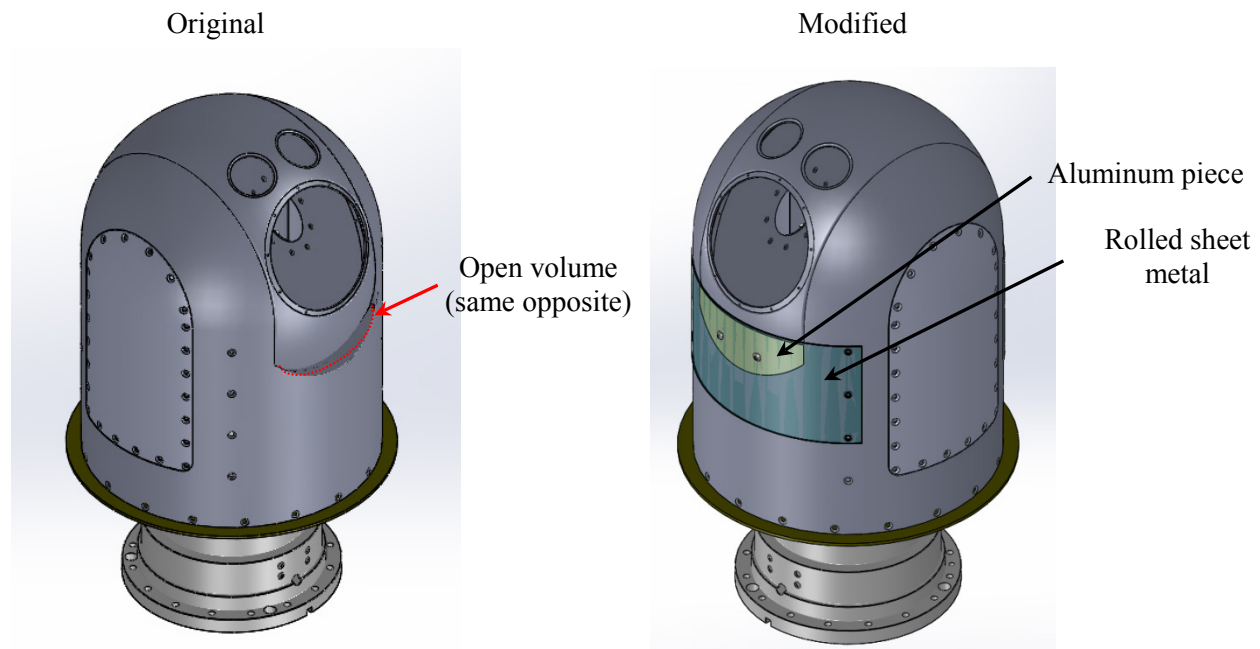


Figure 17. Left: Geometry of original AAOL turret with crescent shaped open volumes at elevation angles of 0 and 180 degrees; Right: AAOL turret modified into canonical geometry.

In addition to our baseline turret modified from its configuration in the AAOL as described above, a new larger-diameter, larger-aperture turret is presently being designed. The new turret will be a somewhat larger turret closer to full-scale turrets being contemplated in prototype systems. This will produce disturbances that are correct amplitude and frequencies for notional prototype systems, which will make real-time adaptive optic experiments possible on board the aircraft. The scaling laws are described in Section VII.

Pressure Turret. Another turret was built exclusively to acquire non-optical dynamic-pressure and temperature measurements at discrete points on its surface. This turret has the same features and dimensions as the original AAOL optical-measurement turret. In fact, it uses an exact duplicate of the

shell made for the optical turret. Holes that would normally be covered by glass windows were replaced with solid aluminum blanks. The turret is capable of being rotated in both the azimuth and elevation degrees of freedom manually and independent of each other. This pressure-turret is mounted to a steel frame which is bolted to the optical bench inside the aircraft. See Figure 18. This turret was instrumented with more than 30 Kulites and some thermocouples. It can be outfitted with sensors on its surface for study of flow characteristics in particular areas [15,16].

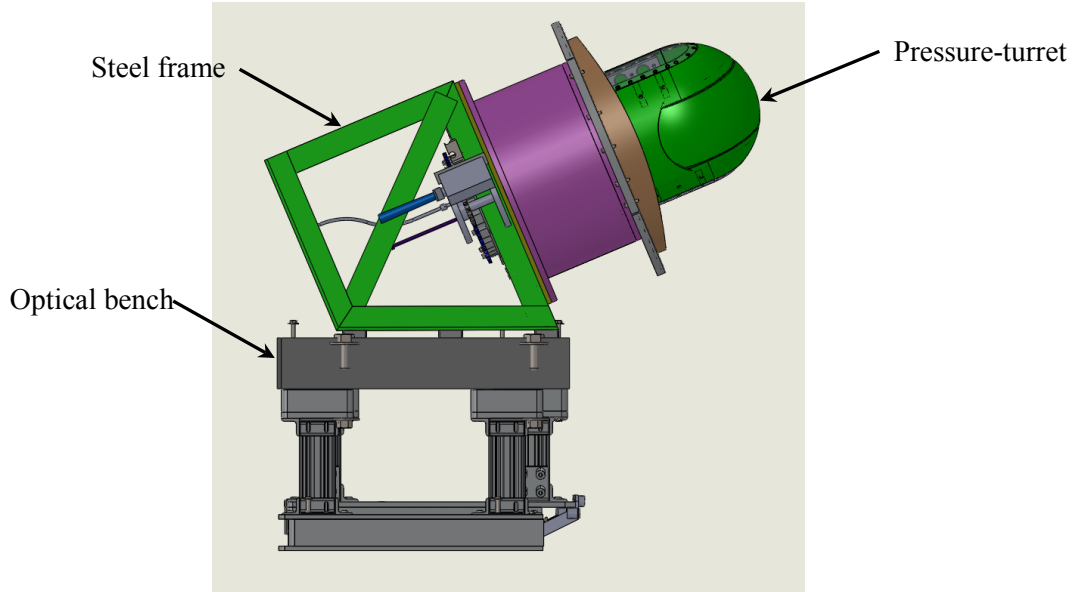


Figure 20. Side-view of solid model of pressure-turret mounted to steel frame bolted to optical bench.

VII. Scaling Laws

Before discussing the aero-optic wavefront scaling laws for different Mach numbers, altitudes and turret size, the way in which we reduce azimuth and elevation information into a single viewing angle and a modified elevation-plane angle needs to be described. Figure 21, Left shows the relationship between these two new angles, (α, β) , to the azimuth, Az , and the elevation, El , angles. These new angles tend to collapse most of the aero-optical data when re-plotted against the viewing angle, α ; the modified elevation angle, β , helps to explain why some of the data does not scale as well as other data because of flow topology, as shown in Figure 21, Right.

The mathematical relationship between the angles is,

$$\alpha = \cos^{-1}[\cos(Az)\cos(El)], \quad \beta = \tan^{-1}\left[\frac{\tan(El)}{\sin(Az)}\right] \quad (2)$$

and the opposite transformation is

$$\begin{aligned} Az &= \tan^{-1}[\tan(\alpha)\cos(\beta)] \\ El &= \sin^{-1}[\sin(\alpha)\sin(\beta)] \end{aligned} \quad (3)$$

While scaling laws for aero-optical data appear in many other papers, it is important to at least mention them here so that the value of the testing on AAOL-T with less-than-full-scale turrets can be properly appreciated; reference [17] is an excellent reference for a more detailed discussion. AAOL and AAOL-T data can be collapsed/scaled in two ways, one that collapses the wavefront OPD_{rms} and OPD

amplitude and modal structure for turret diameter, altitude and flight Mach number, and the second that collapses the frequencies for turret diameter and flight speed.

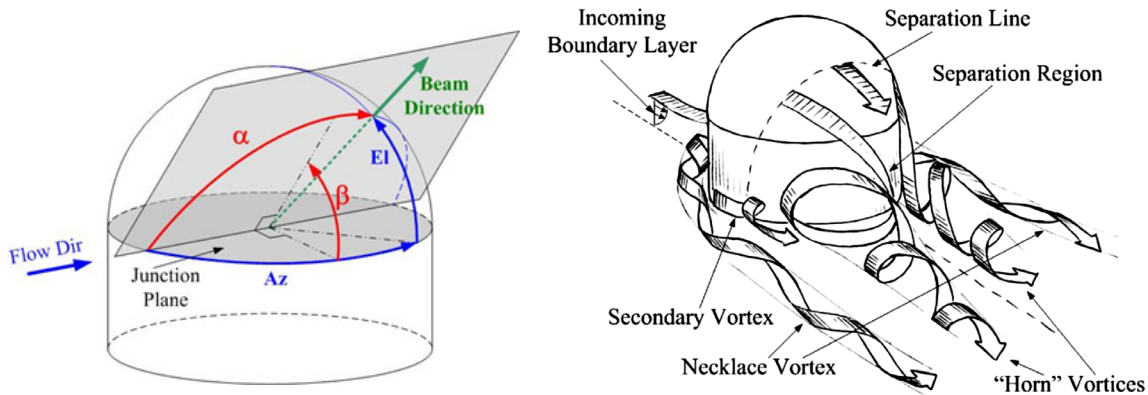


Figure 21. Left: Definitions of Viewing Angle, α and Modified Elevation Plane angle, β ; and Azimuth angle, Az, and Elevation, El. From [8]. Right: Flow topology around a turret at subsonic speeds. From [17].

Amplitude and Modal Structure Scaling. Data taken over many years from different size turrets, flow density and Mach number has shown that the data collapse well using the following scaling law:

$$(\text{OPD}_{\text{rms}})_{\text{NORM}} = \frac{\text{OPD}_{\text{rms}}}{(\rho/\rho_{\text{SL}})M^2 D} \quad (4)$$

or for actual OPD for an individual wavefront,

$$\text{OPD} = \frac{\text{OPD}}{(\rho/\rho_{\text{SL}})M^2 D} \quad (5)$$

where ρ is the density (subscript SL stands for Sea Level), M is the Mach number and D is the diameter of the turret. Equations (4) and (5) make it possible to collect aero-optical data at different Mach numbers and altitude for a given diameter turret and rescale it to different Mach numbers, altitudes and turret diameters. The requirement for scaling depends on geometric similarity of the turret mold line and aperture to turret diameter ratio. Under these constraints, the spatial characteristics of the wavefronts, i.e., modal structure, scales directly with turret diameter, that is to say the spatial patterns of the wavefronts remain the same with respect to the aperture diameter. This remains true for all Mach numbers where the flow is fully subsonic over the turret ($M < \sim 0.6$) as long as the Reynolds number based on the turret diameter is above $\sim 350,000$. Above Mach 0.6 flow over typical turrets becomes supersonic and shocks form over the turret. In these cases, the scaling laws still hold for altitude and turret diameter as long as the Mach numbers are also matched.

Frequency Scaling. The nice thing about AAOL and AAOL-T data is that with the instrumentation described in Section VI, time resolved time series of wavefronts can be collected for use in adaptive-optic studies, for example. The raw data is first collapsed as in Eqs. (2) and (4) so that it can be used for other turret size and flight scenarios as a “time series” of wavefronts at the collection time steps; however, these time steps would not represent the correct steps for the rescaled data. To correct this, the frame rate is first turned into frequency, f , and then collapsed onto Strouhal number, based on turret diameter as:

$$St_D = \frac{f D}{V_\infty} \quad (4)$$

Using the data frame rate, i.e., frequency, the new frequency, i.e., frame rate, for the new application can be found.

As with the amplitude scaling, above \sim Mach 0.6, Mach number makes a difference because of the change in the location of the shock over the turret and depending on the viewing angle, as can be seen in Figure 22. Normalized aperture-averaged wavefront spectra for different viewing angles for several Mach numbers are presented in Figure 22. For the side-viewing angle of $\alpha = 80$ degrees, see Figure 22, Left, the flow is attached over the aperture for $M = 0.5$ and the wavefront spectrum does not have any significant optical features. For $M = 0.6$, a very weak shock appears over the aperture, which results in the appearance of the small peak around $St_D = 1$; otherwise the spectrum stays unchanged. For $M = 0.7$, the shock becomes stronger and the spectrum is significantly increased at low $St_D < 1$. At this Mach number, the spectrum have several peaks, with the dominant ones around $St_D = 0.3$ and 0.18 . For $M = 0.8$, the spectrum has a single peak around $St_D = 0.18$. Recall, that this frequency was associated with the unsteady separation line over the turret [18]. So, these spectra indicate that while at low transonic speeds the shock oscillates at a higher frequency range of $St_D = 0.3..1$, at high transonic speeds, the shock dynamics is locked in with the separation dynamics with a lower frequency; a similar lock-in mechanism was observed around cylindrical turrets. Overall, the spectra for side-viewing angles do not show any collapse between subsonic and transonic speeds.

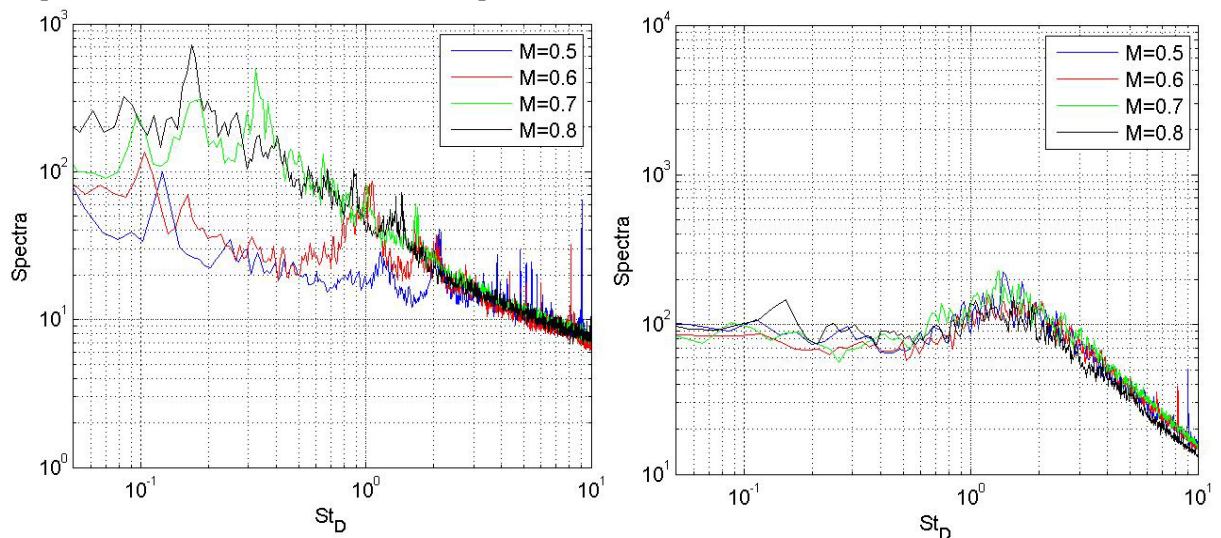


Figure 22. Normalized aperture-averaged wavefront spectra for several Mach numbers for (left) $\alpha = 80$ degrees and (right) $\alpha = 120$ degrees.

For $\alpha = 120$ degree, shown in Figure 22, Right, the beam traverses through the separated region, dominated by the shear-layer structures. Spectra for all Mach numbers, including transonic ones, show a very good collapse. The peak in spectra is around $St_D = 1$, which corresponds to a typical frequency for the shear layer structures at viewing angles near this α . Once the flow is separated, the presence of the shock does not significantly affect the structures in the separation region. Note that for $M = 0.8$ the secondary, separation-line-related peak appears around $St_D = 0.18$; this is also consistent with the lock-in mechanism between the shock and the separation region, discussed above. A detailed discussion of the shock-separation interaction at high transonic speeds is given in [19].

VIII. Example Data and Conclusion

Before concluding this paper, it seems appropriate to give a small sample of data taken at Mach numbers up to Mach 0.8 since data only up to 0.65 has been published for the Citation-based AAOL program. Since modifying the new Falcon 10s, several flight campaigns have been flown, but only two with the AAOL-T turret. The first campaign was conducted in April of 2014, consisted of 4 two-hour formation flights. Optical environment around the flat-window turret was investigated at the following Mach/altitudes: 0.5/15,000, 0.6/18,000, 0.7/26,000 and 0.8/26,000. During this campaign, wavefront measurements were performed using a high-speed Shack-Hartmann wavefront sensor. Similar to the data collection during AAOL program, two different acquisition modes were used for wavefronts: slewing maneuvers and fixed data. Slewing maneuvers involved the laser aircraft moving relative to the laboratory aircraft while wavefronts were continuously acquired; these maneuvers allow for rapid mapping of the optical environment around the turret. Fixed data involved the laser plane maintaining a fixed position with respect to the laboratory aircraft. These acquisitions were performed at a higher sampling rate, as the goal of fixed data acquisitions is to investigate specific flow phenomena with a better temporal resolution. Wavefronts were collected with the spatial resolution of 32x32 subapertures and sample rates of 25 kHz for fixed points and 3 kHz for slewing maneuvers. Simultaneous with the 2-D wavefronts, the overall beam jitter was also measured using a position sensing device. The jitter was acquired along with the turret azimuthal/elevation angle and FSM position information at 25 kHz for 10s. Flight conditions were also recorded with the wavefront and jitter measurements. The aircraft separation was measured using a differential GPS system.

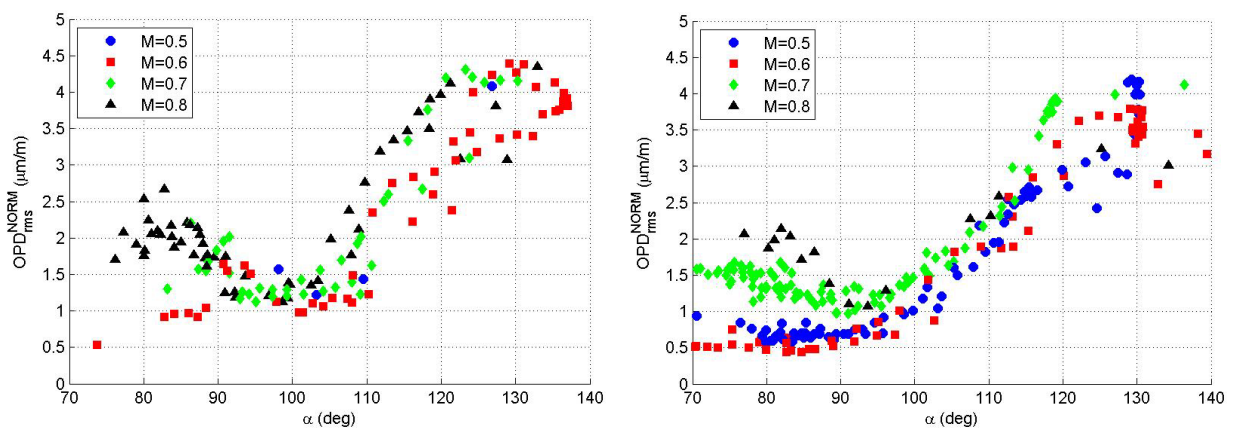


Figure 23. Normalized OPD_{RMS} versus viewing angle for $M = 0.5-0.8$ for the flat-window (left) and conformal-window (right) turret. From [20].

During the second campaign in September of 2014, the turret with both the flat- and the conformal windows was flown in 5 two-hour formation flights at the following Mach/altitudes: 0.5/15,000, 0.6/15,000, 0.6/16,000, 0.7/32,000, 0.7/35,000, 0.7/32,000 and 0.8/35,000 and optical data at both fixed points and slewing maneuvers were collected. During this campaign, wavefronts were collected with a better spatial resolution of 40x40 subapertures and sample rates of 30 kHz for fixed points and 2 kHz for slewing maneuvers. Simultaneous with the 2D wavefronts, the beam jitter was also measured using a position sensing device at 50 kHz for 30 seconds.

Figure 23 shows a summary of overall amounts of aero-optical distortions, OPD_{rms} , normalized by $(\rho/\rho_{SL})M^2D$, for both the flat- and the conformal window turret over a wide range of viewing angles

and several transonic Mach numbers. The presence of the shock of the turret is manifested by the increase of the OPDrms around $\alpha=80$ degrees for $M=0.7$ and $M=0.8$. Another way to visualize the shock is to plot the spatial variation of the wavefronts over the aperture, as the shock creates additional localized distortions. The presence of the shock is visible as a line of the increased distortions, shown in Figure 24. The average shock location is around $\alpha = 80$ degrees and fairly independent of the elevation angle; the streamwise shock extent increases with the Mach number increase. Detailed analysis of the aero-optical data, including the shock dynamics is presented in [20].

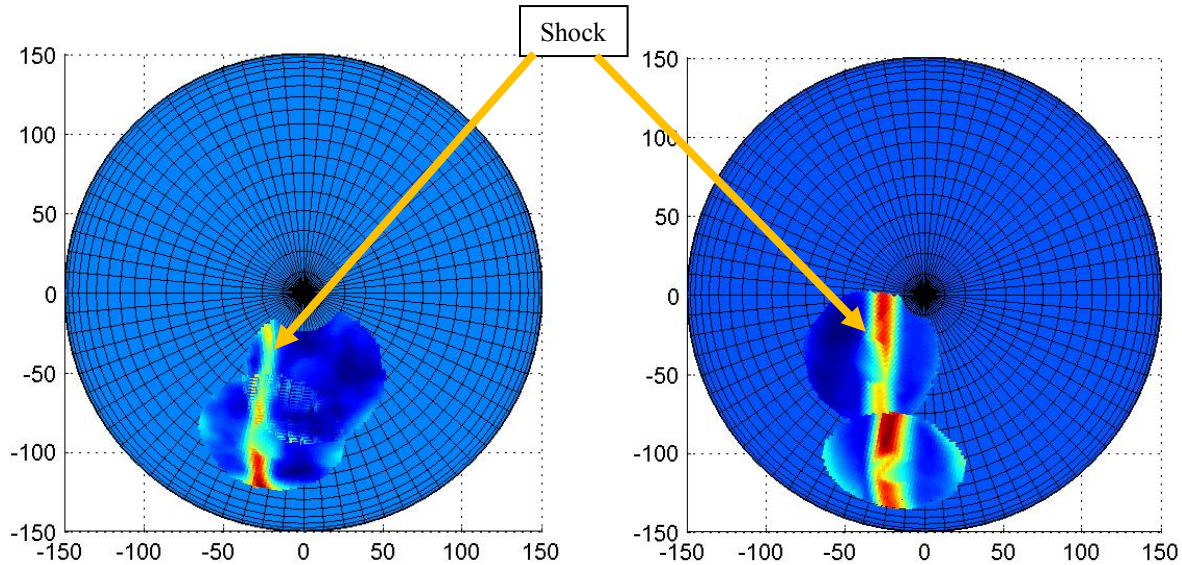


Figure 24. The top view of spatial variation of wavefronts, indicating the shock location for $M=0.7$ (left) and $M=0.8$ (right) for the conformal-window turret. Flow goes from left to right. From [20].

As stated in the Introduction, this paper is intended to describe the new Falcon 10-based AAOL-T flight equipment, procedures data reduction approach. This description ends now with an example of data collected at the higher Mach numbers afforded by the Falcon 10s. In addition to serving as a reference for papers discussing the data taken on the AAOL-T, we hope that enough description of capabilities has been given to entice future users of the program.

Acknowledgments

This work is supported by the Joint Technology Office, Grant number FA9550-13-1-0001. The U.S. Government is authorized to reproduce and distribute reprints for governmental purposes notwithstanding any copyright notation thereon.

References

- [1] R.W. Duffner, *Airborne Laser: Bullets of Light*, Basic Books, Plenum Publishers, New York, 1997.
- [2] E.J. Jumper and E.J. Fitzgerald., "Recent Advances in Aero-Optics," *Progress in Aerospace Sciences*, **37**(3), 299-239 (2001).
- [3] K.G. Gilbert, "The Challenge of High Brightness Laser Systems: a Photon Odyssey," *Opt. Eng.* **52**(7), 071412, 2013.

- [4] N. Bloembergen, et. al., "Lasers, Chapter 3," *Reviews of Modern Physics*, **59**(3), part II, pp. S33-S68, 1987.
- [5] K.J. Gilbert and L.J. Otten (eds), Aero-Optical Phenomena, *Progress in Astronautics and Aeronautics*, Vol. 80, AIAA, New York, 1982.
- [6] M. Wang, A.Mani and S. Gordeyev, "Physics and Computation of Aero-Optics", *Annual Review of Fluid Mechanics*, Vol. 44, pp. 299-321, 2012.
- [7] V.N. Mahajan, "Strehl ratio for primary aberration in terms of their aberration variance," *J. Opt. Soc. Am.*, Vol. 73, pp. 860-861, (1983).
- [8] C. Porter, S. Gordeyev and E. Jumper, "Large-Aperture Approximation for Not-So-Large Apertures," *Optical Engineering*, **52**(7) 071417, 2013.
- [9] Hugo, R.J. and Jumper, E.J., "Experimental Measurement of a Time-Varying Optical Path Difference using the Small-Aperture Beam Technique," *Applied Optics*, 35(22), pp. 4436-4447, 1996.
- [10] R.J. Hugo, E.J. Jumper, G. Havener, and C. Stepanek, "Time-Resolved Wave front Measurements through a Compressible Free Shear Layer," *AIAA Journal* , **35**(4), pp. 671-677 (1997).
- [11] E.J. Fitzgerald and E.J. Jumper, "Aperture Effects on the Aerooptical Distortions Produced by a Compressible Shear Layer," *AIAA Journal*, **40**(2), pp. 267-265 (2012).
- [12] E.J. Fitzgerald and E.J. Jumper, "The Optical Distortion Mechanism in a Nearly Incompressible Free Shear Layer," *Journal of Fluid Mechanics*, **512**, pp. 153-189, 2004.
- [13] E.J. Jumper, MA. Zenk, S. Gordeyev, D. Cavalieri and M.R. Whiteley, " Airborne Aero-Optics Laboratory," *Optical Engineering*, **52**(7), 071408, July 2013.
- [14] Krizo MJ, Cusumano SJ, Fiorino ST, et al,2013:" Design, development, and in-flight testing of a pointer/tracker for in-flight experiments to measure aero-optical effects over a scaled turret" *Opt. Eng.* Vol 52, No. 7, 071415.
- [15] S. Gordeyev, N. De Lucca, E. Jumper, K. Hird, T.J. Juliano, J.W. Gregory, J. Thordahl and D.J. Wittich, " Comparison of Unsteady Pressure Fields on Turrets with Different Surface Features using Pressure Sensitive Paint ", *Experiments in Fluids*, 55, p. 1661, 2014.
- [16] N. De Lucca, S. Gordeyev, E. Jumper, "Global Unsteady Pressure Fields Over Turrets In-Flight", AIAA Paper 2015-0677, 2015.
- [17] S. Gordeyev and E. Jumper, "Fluid dynamics and aero-optics of turrets," *Progress in Aerospace Sciences*, **46**(8),pp. 388-400 (2010).
- [18] S. Gordeyev, N. De Lucca, E.J. Jumper, K. Hird, T.J. Juliano, J.W. Gregory, J. Thordahl and D.J. Wittich, " Comparison of Unsteady Pressure Fields on Turrets with Different Surface Features using Pressure Sensitive Paint ", *Experiments in Fluids*, **55**, p. 1661, 2014.
- [19] A. Vorobiev, S. Gordeyev, E. Jumper, S.Gogineni, A. Marruffo and D.J. Wittich, "Low-Dimensional Dynamics and Modeling of Shock-Separation Interaction over Turrets at Transonic Speeds," AIAA Paper 2014-2357.
- [20] J. Morrida, S. Gordeyev, N. De Lucca, E. Jumper, "Aero-Optical Investigation of Transonic Flow Features And Shock Dynamics on Hemisphere-On-Cylinder Turrets", AIAA Paper 2015-0676, 2015.